



# Cap mesenchyme cell swarming during kidney development is influenced by attraction, repulsion, and adhesion to the ureteric tip

Alexander N. Combes <sup>a,b,✉\*</sup>, James G. Lefevre <sup>c</sup>, Sean Wilson <sup>b</sup>, Nicholas A. Hamilton <sup>c,d</sup>, Melissa H. Little <sup>b,e,✉</sup>

<sup>a</sup> Department of Anatomy & Neuroscience, University of Melbourne, Melbourne 3010 VIC, Australia

<sup>b</sup> Murdoch Childrens Research Institute, Flemington Rd, Parkville, Melbourne, 3052 VIC, Australia

<sup>c</sup> Division of Genomics of Development and Disease, Institute for Molecular Bioscience, The University of Queensland, Brisbane, QLD 4072, Australia

<sup>d</sup> Division of Cell Biology and Molecular Medicine, Institute for Molecular Bioscience, The University of Queensland, Brisbane, QLD 4072, Australia

<sup>e</sup> Department of Paediatrics, The University of Melbourne, Melbourne, 3010 VIC, Australia



## ARTICLE INFO

### Article history:

Received 18 May 2016

Received in revised form

21 June 2016

Accepted 21 June 2016

Available online 23 June 2016

### Keywords:

Kidney development

Cap mesenchyme

Nephron progenitor

Cell migration

Live imaging

## ABSTRACT

Morphogenesis of the mammalian kidney requires reciprocal interactions between two cellular domains at the periphery of the developing organ: the tips of the epithelial ureteric tree and adjacent regions of cap mesenchyme. While the presence of the cap mesenchyme is essential for ureteric branching, how it is specifically maintained at the tips is unclear. Using *ex vivo* timelapse imaging we show that cells of the cap mesenchyme are highly motile. Individual cap mesenchyme cells move within and between cap domains. They also attach and detach from the ureteric tip across time. Timelapse tracks collected for > 800 cells showed evidence that this movement was largely stochastic, with cell autonomous migration influenced by opposing attractive, repulsive and cell adhesion cues. The resulting swarming behaviour maintains a distinct cap mesenchyme domain while facilitating dynamic remodelling in response to underlying changes in the tip.

© 2016 Elsevier Inc. All rights reserved.

## 1. Introduction

Mammalian kidneys function to filter blood and regulate fluid homeostasis in the body through thousands to millions of specialised filtration units called nephrons (Bertram et al., 2011; Merlet-Benichou et al., 1999). Filtrate from this multitude of nephrons is channelled to the bladder through a branched collecting duct system also known as the ureteric tree. The ureteric tree starts as an epithelial outgrowth from the posterior end of the Wolffian duct, which elongates and branches as it grows into the adjacent metanephric mesenchyme (Little and McMahon, 2012). Branching is driven by reciprocal interactions between the tips of the ureteric tree (ureteric tips, UT) and the cap mesenchyme (CM) that surrounds them (Costantini and Kopan, 2010). Factors produced by the CM, including GDNF and FGFs, stimulate proliferation and branching in the underlying tip epithelium while tip-produced factors, including WNT9B, maintain CM identity and also trigger CM differentiation to

form nephrons (Carroll et al., 2005; Karner et al., 2011; Kopan et al., 2014). Each tip-cap domain, together with the surrounding stroma and vasculature, forms a nephrogenic niche. During branching, the mesenchymal population surrounding a given tip must self-renew to provide an ongoing 'cap' for the daughter tips. While lineage tracing definitively shows that a portion of CM cells in any niche 'exit' when induced to commit to nephron formation, it is the balance between nephron commitment and self-renewal that ensures that each niche is maintained to drive subsequent branching and hence ongoing nephron formation. Across development there is a steady reduction in niche size and number of cap and tip cells per niche, however the spatial arrangement of all niche components is maintained. Hence, the CM is only present out at the very periphery of the expanding organ and we do not currently understand how the CM domain is confined to this specific peripheral tip-associated location.

Morphogenesis involves cell movement. Cell movement within the tips of the ureteric epithelium has been documented using live imaging of flattened explant cultures (Chi et al., 2009; Packard et al., 2013; Riccio et al., 2016; Shakya et al., 2005; Watanabe and Costantini, 2004). However, little attention has been paid to cell movement within the CM and this cellular domain is currently described as if it were a static environment. Indeed, previous studies suggest spatially distinct cellular subdomains within the

\*\* Corresponding author at: Department of Anatomy & Neuroscience, University of Melbourne, Melbourne, 3010 VIC, Australia.

\* Corresponding author at: Murdoch Childrens Research Institute, Flemington Rd, Parkville, Melbourne, 3052 VIC, Australia.

E-mail addresses: [alexander.combes@unimelb.edu.au](mailto:alexander.combes@unimelb.edu.au) (A.N. Combes), [melissa.little@mcri.edu.au](mailto:melissa.little@mcri.edu.au) (M.H. Little).

CM based upon differential gene expression, with this proposed to reflect a progressive commitment of cells within each subdomain to a differentiated state (Brown et al., 2013; Mugford et al., 2009). Furthermore, recent papers suggest that exposure to stromal signals around the periphery of the CM domain sensitises CM cells to differentiation (Das et al., 2013; Fetting et al., 2014; Mao et al., 2015). In a static environment, these results imply that peripheral cells are primed to differentiate while those closer to the tip are more likely to self-renew. Likewise, continued association of CM and UT could result from stable cell adhesion between these two domains. We and others recently published live imaging data of limited temporal and spatial resolution, which showed evidence for CM cell movement (Kanda et al., 2014; Lindstrom et al., 2015; Wainwright et al., 2015). The presence of cell motility within the CM raises the question of how a motile population maintains the form and appearance of a coherent domain.

In this study, we have quantitatively analysed patterns of cell movement for > 800 individual cells in the cap mesenchyme using high resolution live imaging of kidney explants from transgenic reporter mice. Extensive cell motility was observed across an 18 h period with cells undergoing a number of previously undescribed behaviours. Cap cells oscillated between periods of 'free movement' and 'attachment' to the adjacent tip. Individual CM cells also dispersed within the niche, interacting with both tip and stromal environments over time and even crossing intervening stromal regions to join another niche. Observations of cell behaviour before and after tip attachment or cell division showed no correlation with changes in cell location or subsequent cell movement that may have indicated a differentiation event in this time window. Mathematical analyses of changes in cell position across time, compared with random movement, showed evidence for three contradictory forces

influencing cell movement; cell adhesion to the tip, cell repulsion from the tip and attraction back to the tip. The balance of these competing forces combines to maintain the form of the CM domain and its relative position as the tip domains grow, split, and re-position during branching morphogenesis.

## 2. Results

### 2.1. The cap mesenchyme is motile during kidney morphogenesis

Kidney explant organ cultures were used to investigate CM cell motility (Costantini et al., 2011). This *ex vivo* culture method has been extensively used to investigate branching morphogenesis (Watanabe and Costantini, 2004), nephron patterning (Lindstrom et al., 2014) and tip cell fate in the developing kidney (Chi et al., 2009; Riccio et al., 2016; Shakya et al., 2005). Importantly, the CM domains in explanted kidneys appropriately associate with tip ends, continue to drive branching morphogenesis, and nephron induction and patterning occurs in an appropriate manner (Lindstrom et al., 2014). *Ex vivo* kidney explants from a CM-specific GFP reporter line (*Six2-TGC<sup>tg/+</sup>*) (Kobayashi et al., 2008) were used for initial timelapse experiments. Low magnification imaging (10x) across 18 h revealed extensive and constant cell movement. Cells migrated within CM domains but also crossed freely between neighbouring domains (Fig. 1A-G, See also Supplementary Movie 1). Heterogeneity in cell speed and distance travelled was clearly apparent. Definitive assessment of CM cell behaviour during kidney development *in vivo* is not feasible with current approaches. However, analysis of *SIX2<sup>+</sup>* cells in fixed 15.5 days post coitum (dpc) embryonic kidneys revealed that numerous individual cap

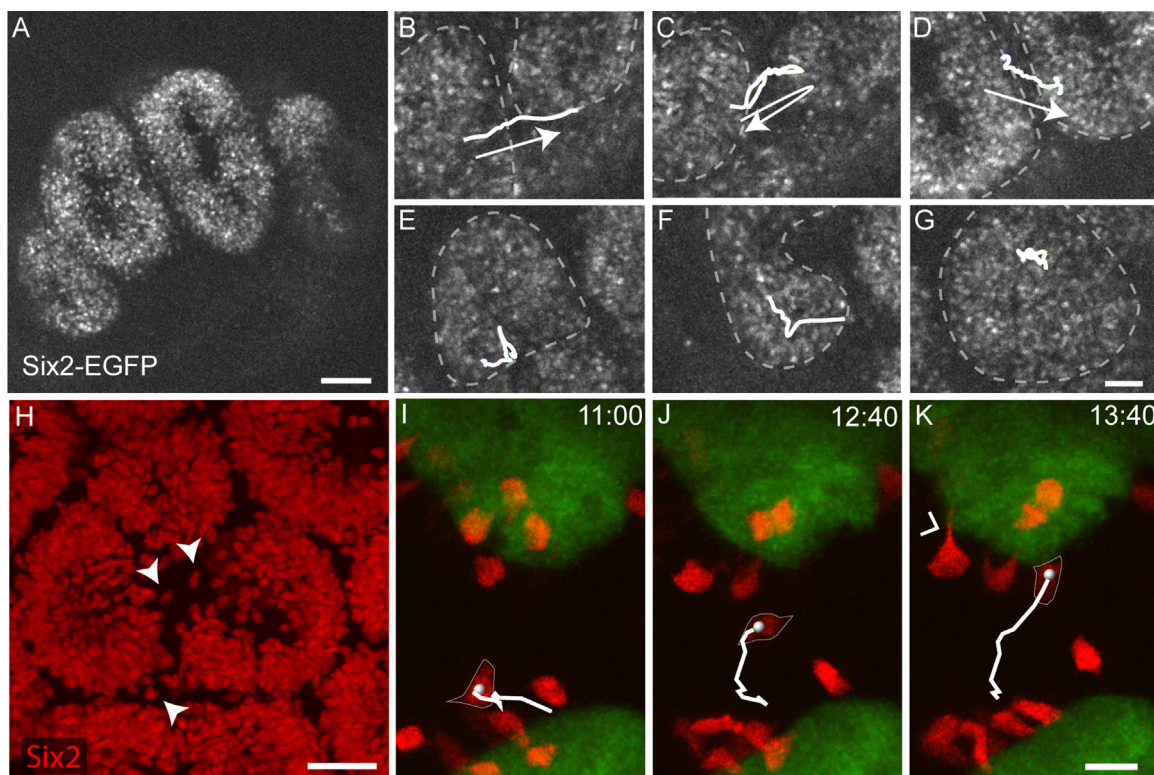


**Fig. 1.** *SIX2<sup>+</sup>* cells migrate within and between CM domains. **A)** 10x confocal image of CM cells marked with nuclear EGFP (white). Scale bar 100 μm. **B-G)** Regions from A. White tracks indicate movement of cells between (B-D) or within (E-G) CM domains across time. Arrows indicate direction of movement. Scale bar for B-G (shown in G) 50 μm. **H)** Isolated *SIX2<sup>+</sup>* cells are seen between domains in fixed 15.5dpc kidneys stained with *SIX2* antibody (red). Scale bar 30 μm. **I-K)** A single CM cell migrates from one *Hoxb7-EGFP* (green) tip to another. Cell is marked with a sphere and outlined in white; track indicates movement in previous time frames. Time is indicated in hh:mm format in the top right corner. Open arrowhead illustrates a slender process extending from one labelled CM cell to touch the adjacent tip. Scale bar for I-K (shown in K) 20 μm.

cells were located between CM domains, supporting the domain-swapping behaviour seen in the *ex vivo* cultures (Fig. 1H).

## 2.2. Quantitative analysis of CM cell movement

Although CM cell movement was clearly evident in the *Six2-TGC<sup>tg/+</sup>* samples, image resolution was not sufficient to unequivocally distinguish between cells at different depths or between cells that crossed paths. Furthermore, it was important to discriminate between cell displacement caused by tissue expansion and authentic cell migration. To overcome these limitations, a subset of cap mesenchyme cells was selectively labelled using a tamoxifen inducible *Six2-cre* (*Six2-GCE/+*) to activate a floxed Tomato (red) fluorescent protein. Tracking of cell movement with respect to the adjacent ureteric epithelium was achieved by visualising tip-expressed *Hoxb7-EGFP*. Imaging in such samples confirmed the niche-swapping of CM cells seen in *Six2-TGC<sup>tg/+</sup>* samples (Fig. 1I-K, Supplementary Movie 2). To quantitatively analyse CM cell migration, tip volumes and individual cap cell positions were defined and tracked across ~18 h of imaging (Fig. 2A-C, Supplementary Movie 3). Data was exported from Imaris into the R statistical programming environment ([www.R-project.org/](http://www.R-project.org/)) (R Core Team, 2015) for analysis, and viewed within a custom visualiser built using Processing 2 (<https://processing.org/>) (Fig. 2D). The complete data set included 852 tracked CM cells from 9 independent samples, including >100 cell division events. Individual cells were only tracked whilst they could be unambiguously identified, hence individual tracks varied in length (mean track duration = 10.32 h). Despite this, a total of 12 cells were tracked through two rounds of division within an 18 h period (mean cell cycle length 12.3 h), suggesting a cell cycle length in line with our previous *in vivo* analyses for this stage of development (fast population cell cycle length of 11.7 h).

## 2.3. The cap mesenchyme tracks with the tip but also shows random movement

Groups of CM cells associated with a single tip showed co-ordinated movement with the tip across time (Fig. 2E, green tracks). Systematic analysis of this behaviour confirmed directed CM cell movement over periods of 10 h or more (Fig. 2G, Supplementary Movie 4). A number of options could explain how CM cells could move with the tip. They may be attracted by a tip secreted factor and maintain their position through directed migration. Conversely, they may be repelled by a tip secreted factor and move along ahead of the tip. CM cells could also be self-adherent (and/or adherent to the tip) and form a mass that is simply pushed along by a growing tip. The possibility of cells being pushed along by the tip was addressed using a custom drift correction approach, which enabled analysis of CM cell movement relative to the closest tip end. A substantial amount of cell movement remained after drift correction (maximum 15% reduction in speed), confirming that CM cells move independent of tip and tissue growth, and independent of each other (Fig. 2F,G). Indeed, moving CM cells extended lamellipodia-like membrane projections characteristic of migrating cells (Fig. 1K arrowhead). Analysis of displacement over time after drift correction suggested that this independent cell migration was not directional (Fig. 2G). While velocity autocorrelation (Fig. 2H) showed some persistence of movement over a short period (<2 h), over longer periods movement was most suggestive of Brownian (random) motion.

Cell movement was highly variable between individual CM cells. Overall analysis of all drift-corrected tracks revealed a wide range of values for speed and distance travelled with no obvious behavioural sub-populations (Supplementary Fig 1). Despite this, there was a significant difference between cells on the two ends of the spectrum. For example, there was a 43 fold difference in the speed of cell migration between the 254 fastest and 254 slowest CM cell

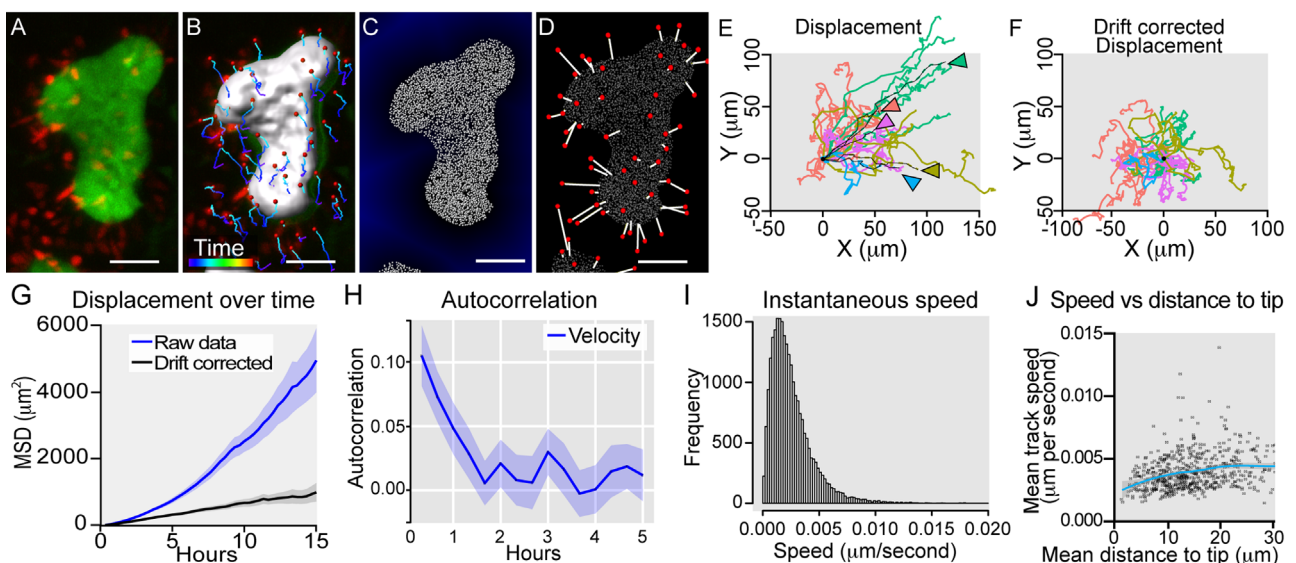


**Fig. 2.** Approach to quantitative analysis of cell migration in the CM. **A**) Single frame from an 18 h movie of CM cells (red) migrating around ureteric tree tips (green). Scale bar 50  $\mu$ m. **B**) Image from A with tip surface rendered in grey and cap cells marked by red spheres. Each spot is connected to a 'track' showing position in previous time points. Tracks coloured by time (scale, bottom left). Scale bar 50  $\mu$ m. **C**) Tip surface from B used to generate a distance transformation (blue gradient) to measure the distance of a CM cell from a tip across time. Volume within the tip surface was filled with points to enable custom analysis. Scale bar 50  $\mu$ m. **D**) Data from B and C visualised in Processing. Cell positions indicated by red spots; tip surface and volume represented by white points; white lines mark shortest distance from cell to tip surface. Scale bar 50  $\mu$ m. **E**) Cell displacement in X and Y before drift correction. Each line represents an individual CM cell and is coloured by the closest tip. Tip displacement is plotted in dashed coloured line with black backbone (indicated by arrowheads of same colour). **F**) Migration trajectories of CM cells after drift correction reveal displacement independent of tip growth and bulk movement. **G**) Plot of mean squared displacement (MSD) over time for CM cell tracks before (blue line) and after (black line) drift correction. Shading indicates 95% confidence interval (CI). An upward curve (raw data) indicates directed movement. A straight line (drift-corrected) indicates undirected movement (Qian et al., 1991). Increasing MSD over time in drift corrected tracks affirms that CM cells move independent of confounding factors. **H**) Velocity autocorrelation shows limited persistence in direction of movement for up to 2 h (drift corrected movement). Shading indicates 95% CI. **I**) Instantaneous speed across all CM cells and timepoints. **J**) Plot of average speed vs. distance to tip indicates that the speed of CM cell migration increases as distance from tip increases from 0 to 20  $\mu$ m. Trend line in blue with shading on either side indicating standard error. Graph cropped at 30  $\mu$ m on X axis.

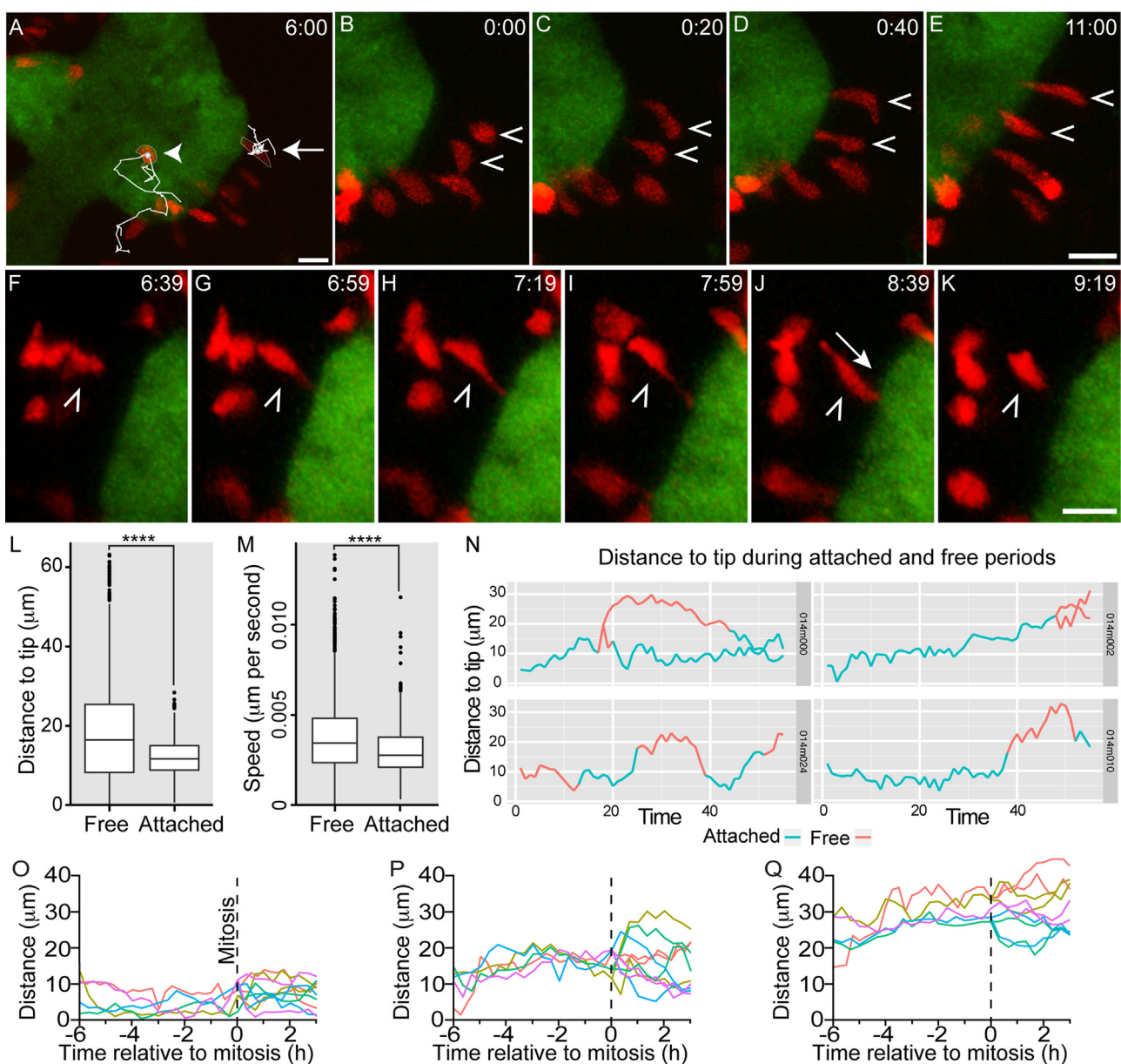


**Fig. 3. CM cells form transient attachments to the ureteric tip.** **A**) Examples of movement patterns for attached (arrow) and unattached (arrowhead) cells across time. White lines indicate cell movement over  $\sim 18$  h. Scale  $20 \mu\text{m}$ . **B-E**) Rounded cells extend processes towards the ureteric tip and adopt an elongated morphology. Time in hh:mm, scale for B-E (displayed in E) is  $20 \mu\text{m}$ . **F-K**) An unattached CM cell (arrowheads) makes contact with the UT through a slim filopodia-like projection in G, which remains stable for over an hour before the cell body is drawn closer to the UT in J (arrow). Two hours after the initial contact this cell detaches from the tip, K. Scale bar for F-K (in K) is  $20 \mu\text{m}$ . **L & M**) Distribution of distance to tip and speed for periods where cells were manually annotated to be attached or free. Box and whisker plots show median, quartiles and outliers under Tukey definition. Mean distance to tip  $12.2 \mu\text{m}$  (attached),  $17.8 \mu\text{m}$  (free), \*\*\*\* $p < 2e-16$  (t-test for difference); mean speed  $2.99e-3 \mu\text{m}/\text{second}$  (attached),  $3.77e-3 \mu\text{m}/\text{second}$  (free), \*\*\*\* $p = 1.9e-15$  (t-test for difference). **N**) Plots of distance to tip across time for four tracked cells and their progeny indicating periods annotated as attached (blue) or free (red). Cells are usually closer to the tip during attached phases. **O-Q**) Plots of distance to tip over time for cells undergoing mitosis. 5 individually coloured representative tracks have been selected to demonstrate distance to tip for  $6$  h prior to mitosis for cells that are (O)  $< 15 \mu\text{m}$  to tip for  $6$  h prior to mitosis, (P)  $< 20 \mu\text{m}$  to tip prior to mitosis, (Q)  $> 20 \mu\text{m}$  to tip for the majority of time prior to mitosis.

movements (1% quantile) (Fig. 2I). Amongst the 325 cells tracked for 10 h or longer, there was a 2.86 fold difference in average speed between the 20 fastest and 20 slowest cells, and a 5.72 fold difference in total displacement over 10 h. After adjusting for variability between experiments, an ANOVA found highly significant heterogeneity in the speed of cell movement ( $p < 2.2e-16$ ), but the differences between cells accounted for only 8.9% of total speed variation. Thus, there was substantial variation in speed across the duration of any individual cell track. There was also an increase in speed of cell migration with increasing distance from the tip surface (Fig. 2J), which is likely influenced by physical interactions with the tip, as discussed later. In short, CM cells move at different speeds to

each other and both speed up and slow down, suggesting that they respond to different environmental cues and/or are affected by various physical forces within their environment across time. This substantial variance in the properties of migrating CM cells was likely to mask underlying principles of movement. We therefore focussed on specific behaviours in detail.

#### 2.4. CM cells form transient attachments to the ureteric tip

Across individual CM tracks, a process of apparent attachment and detachment from the ureteric tip was frequently observed. This process was accompanied by changes in cell morphology.

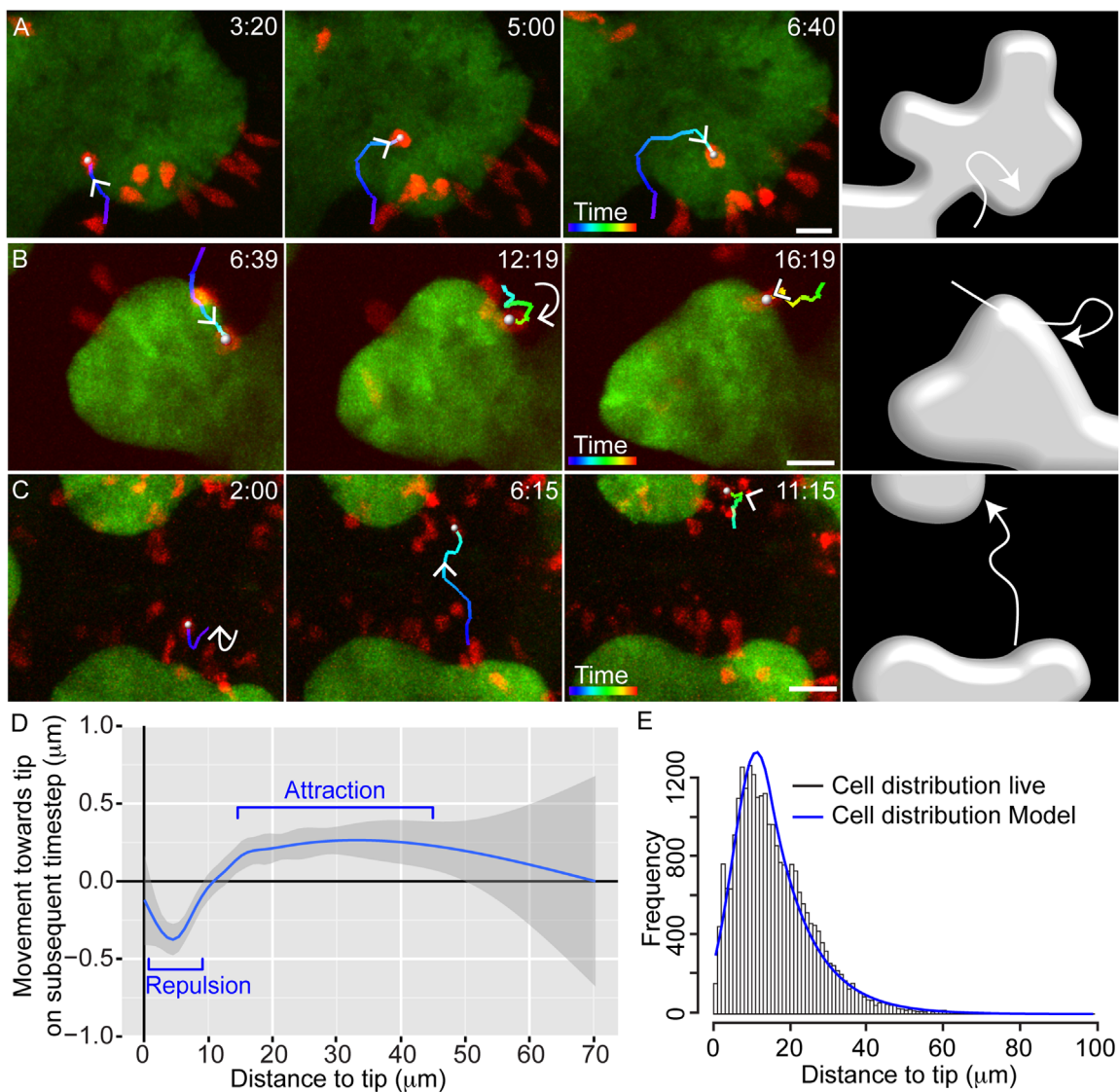


**Fig. 4.** CM migration trajectories suggest attraction to and repulsion from tip. **A)** A CM cell migrates away from the tip edge towards a forming branch point then reorients towards the tip edge. Cell marked with a sphere, migration track coloured by time, arrowheads indicate direction of travel. Scale bar 20  $\mu$ m. Right panel is a cartoon of migration trajectory **B)** Another cell migrates away from the tip edge towards a region of trunk then reorients towards the tip edge. Markings and cartoon as per A, scale 20  $\mu$ m. **C)** A CM cell migrates towards and away from a tip surface then crosses the stroma to reach an adjacent tip. Markings and cartoon as per A, scale 30  $\mu$ m. **D)** Analysis of distance to tip versus movement towards the tip on subsequent timestep. Negative values indicate movement away from the tip, positive values indicate movement towards. A trend line fitted to all data shows a highly significant trend towards movement away from the tip at distances less than 10  $\mu$ m, transitioning to movement towards the tip at distances greater than 15  $\mu$ m (GAM model, shading indicates 95% confidence intervals). **E)** Fit of theoretical CM cell distribution around tip resulting from a steady-state convection-diffusion model of attraction-repulsion forces (blue line) with actual CM cell distribution (histogram).

Some cells located close to the ureteric tip were elongated and displayed constrained movement, consistent with CM cell attachment to that tip (Fig. 3A). Non-attached CM cells appeared more rounded, but elongated once an apparent attachment was made (Fig. 3B-E; Supplementary Movie 5). Elongated cell morphology during ureteric tip tethering was not restricted to the extreme ends of tips but occurred at any location around the tip ampullae (Supplementary Fig 2). As attachment was initiated, cells extended slender processes that appeared to contact the tip before the cell body was drawn closer (Fig. 3B-D, F-K). Over 100 tracks were manually annotated to determine periods where cells appeared to be attached (close to tip, elongated, constrained movement) or freely migrating (more rounded, less constrained). The distance of a CM cell to the tip surface and the speed of migration were both significantly reduced when cells were attached (Fig. 3L-N). Subsequent analysis showed that this attachment effect is sufficient to explain the variation in speed with distance to tip

(Fig. 2J). Most attached cells oscillated between elongated (attached) and rounded (detached) morphologies (Fig. 3F-K). Analysis of all cells near horizontal at the tip ends, and therefore within the higher resolution XY imaging plane, revealed that ~25% of CM cells were attached, rising to 40% when only considering cells <20  $\mu$ m from the tip. The duration of attachment varied from 40 min to 18 h (average = 6.3 h +/- 1.07 h SEM, n=25) and conformed to an exponential distribution (data not shown) consistent with a random process rather than a characteristic period of attachment.

Attachment of a CM cell to the ureteric tip could have affected subsequent cell identity, fate, or behaviour. However, there was no consistent change in cell displacement, location, or speed of migration after attachment (data not shown). We specifically tested whether CM attachment was required for cell division by assessing the distance of mitotic cells to the tip prior to division. Using manually annotated 'attached' vs 'free' periods, the maximum

distance from the tip that an attached cell could reach was 25  $\mu\text{m}$ . The majority of mitotic cells were within 25  $\mu\text{m}$  of the tip up to 6 h prior to mitosis (Fig. 3O-P), in line with the average distribution of all CM cells in these samples. However, several tracks were > 25  $\mu\text{m}$  from the tip surface for up to 6 h prior to mitosis, suggesting that immediate prior interaction with the tip is not required for CM cell division (Fig. 3Q). Furthermore detachment of cells from the tip was not due to cell division as cap cells were observed to detach and reattach to the tip without dividing.

## 2.5. CM cell movement suggests attraction to and repulsion from the ureteric tip

As noted, CM cells migrated independent of one another and were able to swap between cap domains, traversing the intervening stroma to do so. This suggested that cell-cell adhesion within the CM domain does not substantially restrict the movement of CM cells. How then do unattached cells remain associated with the ureteric tip, and how does the CM maintain its position at tip ends? Evidence of directed CM cell movement towards or away from the tip was initially examined qualitatively by observing cell trajectories moving away from the tip at the start of a movie. Some cells migrating in this way were observed to reorient towards a tip domain after migrating past it, consistent with CM cells being attracted to a tip-produced factor (Fig. 4A and B; *Supplementary Movie 6*). Cells migrating away from a tip that entered the stroma reassociated with the original or an adjacent tip (Figs. 1I-K, 4C; *Supplementary Movie 6*). As the speed of cell migration did not change as cells crossed the stroma (data not shown), there is no evidence that the stroma repels CM cells or provides a physical barrier to their migration.

Given the random and independent patterns of CM cell movement observed, retention of the CM at the tip may represent the net result of counteracting repulsive and attractive cues. A systematic analysis of attraction and repulsion was performed by assessing whether cell movement was biased towards or away from the tip surface. While the overall trend in movement was random, a subtle, but highly significant attraction effect was seen at distances greater than 10  $\mu\text{m}$ , transitioning to a similar repulsion at distances less than 10  $\mu\text{m}$  (Fig. 4D). For cells initially at distances greater than 10  $\mu\text{m}$  there was a mean movement towards the tip (attraction; 0.17  $\mu\text{m}$  per time step, median 0.07  $\mu\text{m}$ ;  $p=9.1\text{e-}14$ , *t*-test) whereas net movement away from the tip was observed for cells at distances less than 10  $\mu\text{m}$  from a tip (repulsion; 0.24  $\mu\text{m}$  per time step,

median 0.17  $\mu\text{m}$ ;  $p=3.4\text{e-}16$ , *t*-test). Although these movements toward and away from the tip are relatively subtle, they act to maintain CM cell proximity to the tip as the large random component of motion will tend to cancel out over time. The difference between mean and median values suggests that the attraction/repulsion effects are particularly linked to larger movements. In the case of repulsion, the stronger association with large movements may be due to the attachment state of the cell. The effect of a repulsive cue would be limited by cell attachment, but able to act when cells detach from the tip. For tip distances greater than 15  $\mu\text{m}$ , attraction to tip appears to plateau ( $p=0.99$ , linear regression), suggesting a long-ranged attractive signal. If the force underlying this attraction were to weaken at greater distances then we would expect a change in the trend line, as seen at distances greater than 45  $\mu\text{m}$  (Fig. 4D). To test whether this observed pattern of attraction and repulsion is sufficient to maintain the cap in proximity to the tip, a steady-state convection-diffusion model was fitted to the overall distribution of tip distances (Lefevre et al., 2016). A linear transition from repulsion to attraction was assumed between the tip surface and a distance threshold (fitted value 14.95  $\mu\text{m}$ ), with constant attraction at greater distances. This model was able to reproduce the observed tip distance distribution (Fig. 4E). In particular, this model shows that the exponential drop off in cell numbers at larger tip distances is consistent with a constant attraction to the tip in this domain. These data are consistent with tip-produced cues that both attract unattached CM cells to maintain their association with a niche, and repel unattached CM cells to keep them ahead of the tip as it grows.

## 2.6. Migration drives cell dispersal within the CM

If cells within the CM were spatially positioned within specific subdomains, we may expect to see clonal expansion within those areas after cell division and/or movement of individual CM cells limited to a specific region or distance travelled. In contrast, it appeared that sibling cells dispersed after division (Fig. 5A-C,D-F, *Supplementary Movie 7*). To assess this more comprehensively, 101 cell divisions were analysed to determine whether mitotic siblings remained closely associated or in any way constrained within a particular microenvironment. The average distance between related cells was measured for up to 40 time steps after mitosis. The distance between sibling cells after cytokinesis steadily increased over the first ten time steps to 20  $\mu\text{m}$  (2–4 cell diameters) and continued to increase at a lower rate thereafter

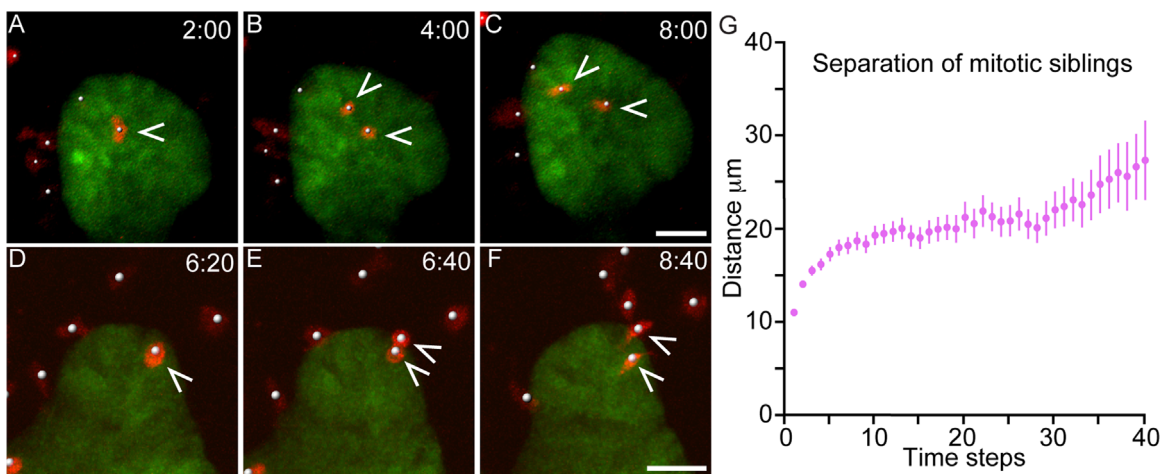


**Fig. 5.** Migration drives cell dispersal within the CM. **A-C)** Separation of siblings from division of a single cell in panel A (arrowheads) across 6 h. Time in hh:mm, scale bar 30  $\mu\text{m}$ . **D-F)** Separation of siblings from division of a single cell in panel D (arrowheads) across 2:20 min. Time in hh:mm, scale bar 30  $\mu\text{m}$ . **G)** Average separation of mitotic siblings after division ( $n > 100$ ), bars indicate SEM.

(Fig. 5G). This dispersal of cells after division argues against restriction of cells within microdomains and is consistent with previous data examining cumulative EdU incorporation experiments in which clonal expansion was not observed in the earlier stages of kidney development.

## 2.7. Individual cap cells interact with both tip and stromal environments over time

Signals from the tip and stroma are proposed to regulate CM cell identity and may also influence cell migration. However, what we observed suggests that CM cells move freely between these two regions and hence should experience signals from both. Some cells migrated across intervening stromal regions to join a distinct CM domain or return to the original CM. Other cells were seen to migrate from positions equidistant to two tips (presumably interacting with stroma) to the tip surface without swapping niches (Fig. 6A–C; Supplementary Movie 8). Rare attached CM cells spanned from tip to stroma in 15.5dpc fresh fixed samples (Supplementary Fig 2). To test how many individual CM cells were likely to experience both tip and stromal environments across time, we defined the dimensions of the CM domains in fixed samples across development (11.5–19.5dpc fixed kidneys; Supplementary Fig 3), and in our live cultures, to determine the boundaries of CM and stroma in terms of distance from the tip. Cell distributions changed over time. From 12.5dpc, the average number of cell layers per CM domain decreased from  $4.7 \pm 2.8$  layers at 12.5dpc to a relatively stable depth of  $2.6 \pm 0.5$  from 14.5dpc to 19.5dpc. After 13.5dpc in vivo, cells further than 25  $\mu\text{m}$  from the nearest tip are likely to be exposed to the stromal environment while cells at <25  $\mu\text{m}$  are likely to interact with the tip (Fig. 6D–E). Using these parameters, 44.6% of CM cells tracked for at least 10 h were likely to interact with both tip and stromal environments (Fig. 6F).

## 2.8. CM commitment does not appear to involve active migration

Classic stem cell niche models, such as the *drosophila* testis stem cell niche, consist of a defined arrangement of stem cells,

transit amplifying cells, and differentiated progeny organised spatially in a linear progression from one state to another (de Cuevas and Matunis, 2011). The CM has also been proposed to have a progression of distinct stages of commitment, from the uninduced *Cited1*<sup>+</sup>*Six2*<sup>+</sup>*Wnt4*<sup>-</sup> self-renewing stem cell to the *Cited1*<sup>-</sup>*Six2*<sup>+</sup>*Wnt4*<sup>+</sup> differentiated state (Mugford et al., 2009). These states are regarded as having distinct spatial locations with the uninduced population closest to the tip and nephron formation occurring down the extending trunk (armpit region) (Brown et al., 2013; Mugford et al., 2009). It has been unclear how an individual CM cell moves from the uninduced region (top) to the site of nephron formation (bottom). Directional migration is one possible mechanism. To test this hypothesis, the maintenance of the three dimensional organisation of the CM in culture was confirmed (Supplementary Fig 4) and cell tracks were analysed for 'top to bottom' movements. Rare individual cells (0.6% of all tracks ( $n=5$ ), 3% in a single sample with deeper imaging (4 cells)) were seen to migrate from the presumed uninduced region towards the site of nephron formation (Fig. 7A, Supplementary Movie 9). An equal number of cells were seen to migrate in the opposite direction (5 cells, 4% in sample with deeper imaging) (Fig. 7B, Supplementary Movie 9), representing movement from a region assumed to induce commitment to a region of self-renewal. This analysis did not reveal a trend of directed movement towards the site of nephron formation and demonstrates that some CM cells are not confined within specific cellular subcompartments. Longer term imaging experiments will be required to clarify the extent of movement between proposed domains within the CM.

## 3. Discussion

This study aimed to assess the dynamics of CM cell behaviour to better understand kidney morphogenesis. Our analysis of over 800 CM cells in embryonic kidney explants revealed an unexpected amount of cell movement. Across an 18 h period, a single CM cell can move such that it interacts with both tip and stroma, attaches and detaches from an adjacent ureteric tip, and can even leave one CM domain and move to another. This constant

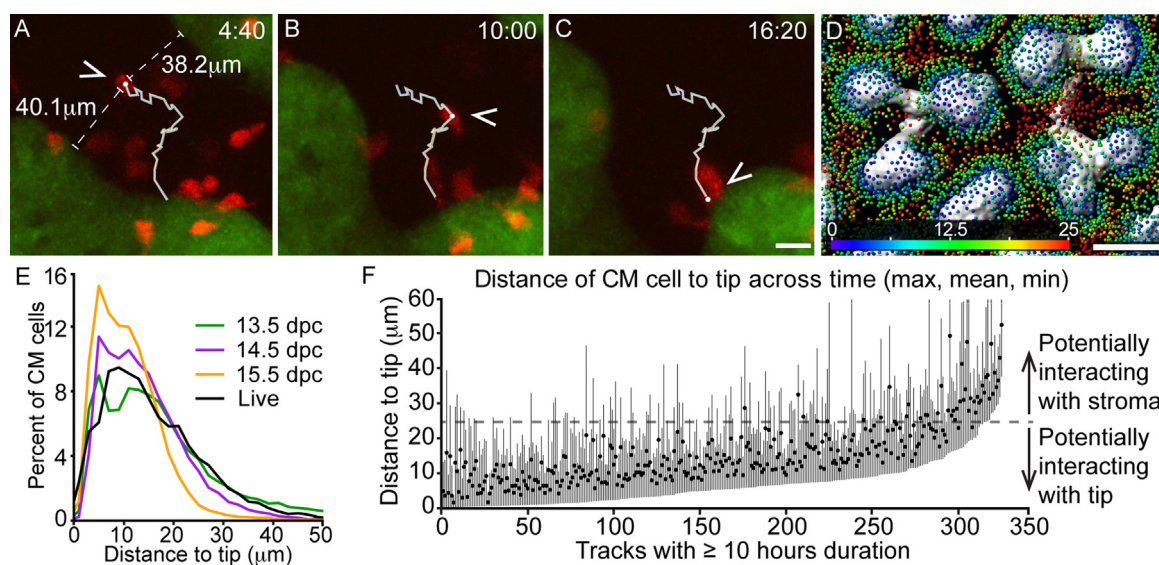


**Fig. 6.** Migration enables individual CM cells to interact with both tip and stromal environments over time. **A–C** A CM cell equidistant from two adjacent tips (arrowheads) migrates to a tip surface. Time in hh:mm, scale bar for all (displayed in C) is 20  $\mu\text{m}$ . **D**) Distribution of CM cells from 14.5dpc tip surface (grey). CM cell nuclei (spheres) are coloured by distance from tip (scale in bottom left). Scale bar 50  $\mu\text{m}$ . **E**) Histograms showing the distance of CM cells to the tip surface at 13.5–15.5dpc from fresh fixed mouse kidneys and the live data set. **F**) Graph of distance to tip for CM cell tracks of > 10 h duration. Spots represent the average distance from tip across an entire track, the top of each bar represents the maximum distance from the tip and the bottom of each bar is the minimum distance from the tip across time.

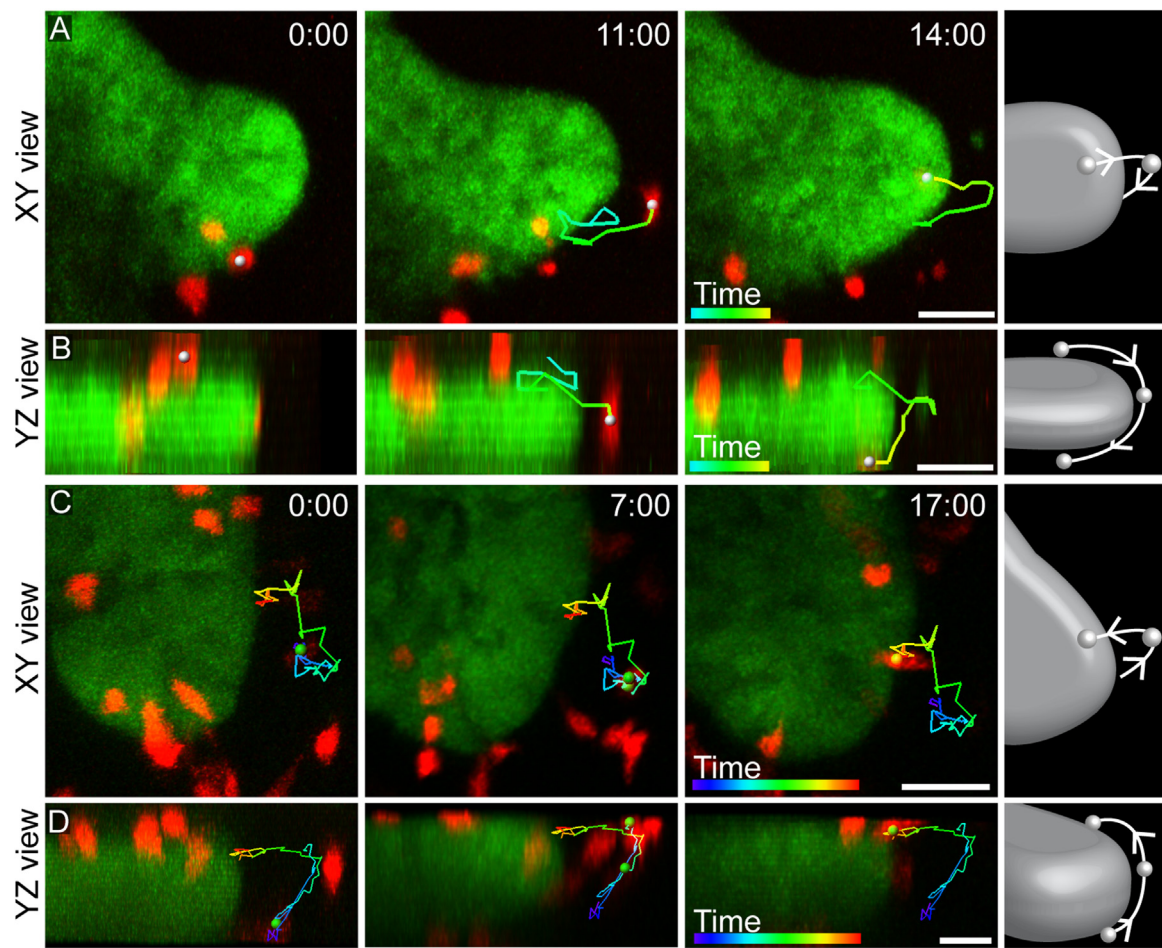


**Fig. 7.** CM cells cross proposed domain boundaries. **A)** XY and YZ views of a CM cell that migrates from the “top” of the tip to the site of nephron formation across 14 h. Cartoon summary of movement on right side. Time in hh:mm. Track coloured by time, indicated by scale in bottom left of last data panel. Scale bars are 30  $\mu\text{m}$  and apply to all images. **B)** XY and YZ views of a CM cell that migrates from under the tip to the top of the sample. Cartoon summary of movement on right side. Time in hh:mm. Track is coloured by time, indicated by scale in bottom left of last data panel. Scale bar for all XY images (shown in last data panel) is 30  $\mu\text{m}$ . Scale bar for all Z images is 20  $\mu\text{m}$ .

movement results in rapid dispersal of sibling cells after division and causes general intermixing of the CM, preventing formation of clonal patches of cells. CM cells appear to move freely throughout the CM region and can move both towards and counter to the direction of assumed differentiation. This broad pattern of cell movement is best described as the stochastic and cell-autonomous interpretation of multiple conflicting signals. Similar to that of swarm behaviour, the net outcome of this apparently chaotic movement is the maintenance of an identifiable population.

CM domains remain tightly associated with tips as they grow and branch. In this study, we show that some CM cells are physically attached to the UT and passively moving with the tip during branching or elongation. However, these attachments are transient (mean duration  $\sim 6$  h) with a substantial proportion of the CM unattached at any point in time. While unattached, these cells can theoretically disperse. However, we show statistical evidence of signals for both attraction to and repulsion from the tip. Further evidence for CM cell attraction to UT has recently been provided from time lapse imaging cultures of re-associated kidney cells (Leclerc and Costantini, 2016). A balance between the counteracting signals of attraction and repulsion presumably maintains the CM around a tip whilst allowing the flexibility to reshape in response to tip branching. While the nature of any such signals is not known, knockout of the Slit ligand receptor, *Robo2*, which is expressed in the CM, results in mislocalisation of CM cells down the trunk and the presence of ureteric tips within the centre of the organ (Wainwright et al., 2015), pointing to a potential role for ROBO/SLIT

signalling in CM cell repulsion. While analysis of cell migration in this *Robo2* null background concluded no overall change in CM movement, this was performed at low resolution with no drift correction or capacity to track migration trajectories with respect to the tip, and therefore was not definitive. It remains possible that ROBO2-mediated signalling contributes to CM cell repulsion but that remaining signals in the null mouse are sufficient to maintain a CM domain, albeit mislocalised compared to controls.

In the current static model, cell position within the CM domain reflects degree of commitment to differentiation, with differential responses to signals from tip and stroma (Das et al., 2013; Fetting et al., 2014). At the developmental timepoint investigated in these studies, the CM is approximately 3 cell layers (25–30  $\mu\text{m}$ ) thick. While different layers of cells could experience differential exposure to stromal versus tip signals, some elongated CM cells were observed to span this entire distance. In addition, our data shows that migration allows CM cells to interact with both tip and stromal environments over time. Hence, each cell must balance input from potentially opposing signals. The relative amount of time a cell spends interacting with the tip or the stroma may still influence the decision to differentiate. In support of this, ablation of the stroma or stroma-expressed *Fat4* appeared to increase the size of the CM, which has been interpreted as an impairment of CM differentiation (Bagherie-Lachidan et al., 2015; Das et al., 2013). In this study, we observed that during phases where CM cells are not attached to the tip they have the capacity to move within the CM domain or move between adjacent domains. The fact that CM cells

return to their original niche or an adjacent niche after entering a field of stromal cells suggests chemotaxis towards the tip or back to other CM cells. Indeed, the absence of CM domains not associated with tips suggests a major role for CM-tip attraction. Alternatively, this behaviour could result from a reduced capacity for a CM cell to remain within the stromal environment. However, migration trajectories do not slow as cells ingress into the stroma, implying that the CM-stromal boundary is less likely to be maintained by stromal repulsion. In addition, the mode of cell movement does not appear to change during a stromal 'crossing', so we assume that it is still primarily driven by CM cell migration rather than adhesion-based cell exclusion.

The individual signals driving each of the responses observed (adhesion, repulsion, attraction) are yet to be identified, however many mutant mice display phenotypes in which maintenance of the CM domain across development is affected (Kopan et al., 2014). To date, none of these have been analysed with respect to an effect on cell movement. Recent single cell RNA profiling analyses suggest considerable heterogeneity between individual CM cells (Chen et al., 2015), as might be expected in such a dynamic system. That study also observed that the phenotype of cells within the CM changes across development, but that returning an 'old' CM cell into the CM domain of a 'young' niche can change its behaviour with respect to self-renewal potential (Chen et al., 2015). Furthermore, 'old' cells were less likely to be retained in a young niche, implying a mechanism for selective depletion such as an inability to respond to migration cues or exclusion from the CM through a change in cell-cell adhesion. Indeed CM aging was associated with changes in cell-cell adhesion and Fgf20 signalling. We have also observed increased evidence for clonal patch formation within the CM as development progresses. These changes in CM gene expression and adhesion across time are likely to correlate with changes in CM cell migration, and may point to some of the regulators of CM morphology.

In conclusion, the data presented here represents a significant revision of the way we consider the structure of the cap mesenchyme. What was formerly considered a static cellular environment has proven to be dynamic. Continuous cell movement within the niche results in a constant change in the likely signalling environment of any given CM cell. As a result, the niche may not be neatly segregated into spatial subdomains required for a linear differentiation of CM cells to an induced fate. Each CM cell is being simultaneously repelled from the tip, attached to the tip and attracted to tip. These competing forces facilitate the dynamic remodelling required to maintain a domain around the ureteric tips, which is vital for continued branching and nephron induction. Understanding, and hence manipulating, these signals may allow the prolongation of CM self-renewal, and consequently ureteric branching, to optimise kidney development.

## 4. Materials and methods

### 4.1. Mouse Strains and selective labelling of cap mesenchyme cells

Live imaging was performed with *Six2-TGC<sup>tg/+</sup>* (EGFP-CRE driven by the *Six2* promoter; Mouse genome informatics (MGI) strain name: Tg(*Six2*-EGFP/cre)1Amc) (Kobayashi et al., 2008); *Six2<sup>GCE/+</sup>* (EGFP-CRE-ERT2 inserted into the *Six2* locus; MGI: *Six2*<sup>tm3(EGFP/cre/ERT2)Amc</sup>) (Kobayashi et al., 2008); *Hoxb7-EGFP* (EGFP driven by the *Hoxb7* promoter; MGI: Tg(*Hoxb7*-EGFP)33Cos) (Srinivas et al., 1999) and Tomato (Cre-activated tdTomato fluorescent protein in the *Rosa26* locus; MGI: Gt(ROSA)26Sor<sup>tm1(CAG-tdTomato)Hze</sup>) (Madisen et al., 2010). Selective CM cell labelling was achieved by incubating 12.5dpc *Six2<sup>GCE/+</sup>*/*Hoxb7-EGFP*/tdTomato kidneys in 0.1uM solution of Ethanol-suspended 4OHT (Sigma

H6278) in CO2 independent media (Life Technologies 18,045–088) for 40 min at room temperature then rinsing 3 times prior to overnight culture. Tomato expression was detected 10–12 h after 4OHT treatment.

### 4.2. Kidney culture and live imaging

Kidneys were cultured as previously described (Costantini et al., 2011) and imaged ~24 h after induction. Samples were imaged on inverted confocal microscopes (Zeiss 710 and 780) using 10x air, or 40x long working distance water immersion objectives. Laser power, scan time, Z-sampling, and time intervals between successive images were optimised to balance phototoxicity with resolution. 15 or 20 min intervals were used, most movies were taken over ~18 h. Times displayed in movie figure panels are relative to the start of the timelapse in hh: mm format.

### 4.3. Antibodies, immunofluorescence, and fixed imaging

The following primary antibodies were used: mouse anti-calbindin D28K (Sigma-Aldrich C9848), mouse anti-cytokeratin (Abcam Ab11213 and Ab115959), rabbit anti-SIX2 (Proteintech 11,562–1-AP). Alexa Fluor-conjugated secondary antibodies (Life Technologies) were used to detect the primary antibodies and DAPI (Sigma-Aldrich D8417) was used at 1:2000 to label nuclei. Whole mount immunofluorescence was carried out according to published protocols (Combes et al., 2014).

### 4.4. Image analysis and cell tracking

Primary image analysis and cell tracking was performed in Imaris (Bitplane). Cells within *Six2-TGC<sup>tg</sup>* data were manually tracked on the basis of higher than average GFP intensity and autocorrelation in cell movement. Data from *Six2<sup>GCE/+</sup>*/*Hoxb7-EGFP*/Tomato explants was processed as follows: signal from the *Hoxb7-EGFP* channel was used to make a tip surface, which was used to generate a distance transformation, and define a spots-based representation of tip volumes in 3D. Tip ends were manually tracked for use in drift correction. CM cells were identified and manually tracked using the spots function. Cells were tracked from the earliest to the latest timepoint in which they could be individually identified. Tracks for cells that could only be followed for a few timepoints were discarded. All data was exported from Imaris as.csv files.

### 4.5. Drift correction and statistical analysis

As drift correction was required for files containing multiple tips that were growing in different directions, a custom post-hoc protocol was developed in which the movement of each CM cell in each interval between consecutive time points was adjusted by subtracting the weighted average of the tip end track movements in the same interval. Weights were the inverse square distance between the cell and tip at the given time. When the niche of a CM cell was unambiguous, this algorithm assigned predominant weight to the associated tip track, while providing smooth transitions when the niche was ambiguous or changed over time. Drift correction was applied to horizontal movement only.

All track branchpoints were identified, and used to separate data into unbranched tracks for analysis and to compare migration of mitotic siblings. Drift-corrected migration was quantified by instantaneous speed, estimated from single time step movements, and by displacement over longer time scales (measured as straight-line distance from start position). Directionality of movement was assessed using mean squared displacement (MSD) and velocity autocorrelation. See (Lefevre et al., 2016) for details of quantitative methods and statistical tests including a summary of

the data, and methods for calculation of mean squared displacement, heterogeneity in cell speed, attachment, and attraction/repulsion.

## Author contributions

A. N. C was involved in designing and performing the experiments, cell tracking, Imaris-based analysis, collation, interpretation, and presentation of the data, and substantially contributed to writing of the manuscript. J. L was involved in the development of mathematical and statistical analysis, interpretation, collation and presentation of the data, and writing the manuscript. S. W. was involved in data collection and presentation. N. A. H supervised and was involved in the development of mathematical and statistical analysis, presentation and writing the manuscript. M. H. L. was responsible for the initial concept of the project, and was involved in the design of experiments, analysis and interpretation of the data, and substantial writing of the manuscript. All authors contributed to editing the manuscript.

## Acknowledgements

This work was supported by the Australian Research Council (DE150100652), the National Health and Medical Research Council of Australia (APP1002748, APP1063696), and the Human Frontiers in Science Program (RGP0039/2011). Microscopy was performed at the ACRF/IMB Cancer Biology Imaging Facility, which was established with the support of the Australian Cancer Research Foundation, and at the Murdoch Childrens Research Institute. A. N. C. holds a Discovery Early Career Researcher Award from the Australian Research Council (DE150100652). M. H. L. is a Senior Principal Research Fellow of the NHMRC (APP1042093). We thank Frank Costantini and Cristina Cebrian for assistance in establishing live imaging methods and Adler Ju for technical support. The authors declare no competing financial interests.

## Appendix A. Supplementary material

Supplementary data associated with this article can be found in the online version at <http://dx.doi.org/10.1016/j.ydbio.2016.06.028>.

## References

- Bagherie-Lachidan, M., Reginensi, A., Pan, Q., Zaveri, H.P., Scott, D.A., Blencowe, B.J., Helmbacher, F., McNeill, H., 2015. Stromal Fat4 acts non-autonomously with Dchs1/2 to restrict the nephron progenitor pool. *Development* 142, 2564–2573.
- Bertram, J.F., Douglas-Denton, R.N., Diouf, B., Hughson, M.D., Hoy, W.E., 2011. Human nephron number: implications for health and disease. *Pediatr. Nephrol.* 26, 1529–1533.
- Brown, A.C., Muthukrishnan, S.D., Guay, J.A., Adams, D.C., Schafer, D.A., Fetting, J.L., Oxburgh, L., 2013. Role for compartmentalization in nephron progenitor differentiation. *Proc. Natl. Acad. Sci. USA* 110, 4640–4645.
- Carroll, T.J., Park, J.S., Hayashi, S., Majumdar, A., McMahon, A.P., 2005. Wnt9b plays a central role in the regulation of mesenchymal to epithelial transitions underlying organogenesis of the mammalian urogenital system. *Dev. Cell* 9, 283–292.
- Chen, S., Brunsell, E.W., Potter, S.S., Dexheimer, P.J., Salomonis, N., Aronow, B.J., Hong, C.I., Zhang, T., Kopan, R., 2015. Intrinsic Age-Dependent Changes and Cell-Cell Contacts Regulate Nephron Progenitor Lifespan. *Dev. Cell* 35, 49–62.
- Chi, X., Michos, O., Shakya, R., Riccio, P., Enomoto, H., Licht, J.D., Asai, N., Takahashi, M., Ohgami, N., Kato, M., Mendelsohn, C., Costantini, F., 2009. Ret-dependent cell rearrangements in the Wolffian duct epithelium initiate ureteric bud morphogenesis. *Dev. Cell* 17, 199–209.
- Combes, A.N., Short, K.M., Lefevre, J., Hamilton, N.A., Little, M.H., Smyth, I.M., 2014. An integrated pipeline for the multidimensional analysis of branching morphogenesis. *Nat. Protoc.* 9, 2859–2879.
- Costantini, F., Kopan, R., 2010. Patterning a complex organ: branching morphogenesis and nephron segmentation in kidney development. *Dev. Cell* 18, 698–712.
- Costantini, F., Watanabe, T., Lu, B., Chi, X., Srinivas, S., 2011. Dissection of embryonic mouse kidney culture in vitro, and imaging of the developing organ. *Cold Spring Harb. Protoc.*, 613. <http://dx.doi.org/10.1101/pdb.prot5613>.
- Das, A., Tanigawa, S., Karner, C.M., Xin, M., Lum, L., Chen, C., Olson, E.N., Perantoni, A.O., Carroll, T.J., 2013. Stromal–epithelial crosstalk regulates kidney progenitor cell differentiation. *Nat. Cell Biol.* 15, 1035–1044.
- de Cuevas, M., Matunis, E.L., 2011. The stem cell niche: lessons from the *Drosophila* testis. *Development* 138, 2861–2869.
- Fetting, J.L., Guay, J.A., Karolak, M.J., Iozzo, R.V., Adams, D.C., Maridas, D.E., Brown, A.C., Oxburgh, L., 2014. FOXD1 promotes nephron progenitor differentiation by repressing decorin in the embryonic kidney. *Development* 141, 17–27.
- Kanda, S., Tanigawa, S., Ohmori, T., Taguchi, A., Kudo, K., Suzuki, Y., Sato, Y., Hino, S., Sander, M., Perantoni, A.O., Sugano, S., Nakao, M., Nishinakamura, R., 2014. Sall1 maintains nephron progenitors and nascent nephrons by acting as both an activator and a repressor. *J. Am. Soc. Nephrol.* 25, 2584–2595.
- Karner, C.M., Das, A., Ma, Z., Self, M., Chen, C., Lum, L., Oliver, G., Carroll, T.J., 2011. Canonical Wnt9b signaling balances progenitor cell expansion and differentiation during kidney development. *Development* 138, 1247–1257.
- Kobayashi, A., Valerius, M.T., Mugford, J.W., Carroll, T.J., Self, M., Oliver, G., McMahon, A.P., 2008. Six2 defines and regulates a multipotent self-renewing nephron progenitor population throughout mammalian kidney development. *Cell Stem Cell* 3, 169–181.
- Kopan, R., Chen, S., Little, M., 2014. Nephron progenitor cells: shifting the balance of self-renewal and differentiation. *Curr. Top. Dev. Biol.* 107, 293–331.
- Leclerc, K., Costantini, F., 2016. Mosaic analysis of cell rearrangements during ureteric bud branching in dissociated/reaggregated kidney cultures and in vivo. *Dev. Dyn.* 245, 483–496.
- Lefevre, J.C., Combes, A.N., Little, M.H., Hamilton, N.A., 2016. Analysis of cap mesenchyme cell migration during kidney development. Data in Brief, <http://dx.doi.org/10.1016/j.dib.2016.08.053>.
- Lindstrom, N.O., Carragher, N.O., Hohenstein, P., 2015. The PI3K pathway balances self-renewal and differentiation of nephron progenitor cells through beta-catenin signaling. *Stem Cell Rep.* 4, 551–560.
- Lindstrom, N.O., Lawrence, M.L., Burn, S.F., Johansson, J.A., Bakker, E.R., Ridgway, R.A., Chang, C.H., Karolak, M.J., Oxburgh, L., Headon, D.J., Sansom, O.J., Smits, R., Davies, J.A., Hohenstein, P., 2014. Integrated beta-catenin, BMP, PTEN, and Notch signalling patterns the nephron. *Elife* 4, e04000.
- Little, M.H., McMahon, A.P., 2012. Mammalian kidney development: principles, progress, and projections. *Cold Spring Harb. Perspect. Biol.*, 4.
- Madisen, L., Zwingman, T.A., Sunkin, S.M., Oh, S.W., Zariwala, H.A., Gu, H., Ng, L.L., Palmiter, R.D., Hawrylycz, M.J., Jones, A.R., Lein, E.S., Zeng, H., 2010. A robust and high-throughput Cre reporting and characterization system for the whole mouse brain. *Nat. Neurosci.* 13, 133–140.
- Mao, Y., Francis-West, P., Irvine, K.D., 2015. Fat4/Dchs1 signaling between stromal and cap mesenchyme cells influences nephrogenesis and ureteric bud branching. *Development* 142, 2574–2585.
- Merlet-Benichou, C., Gilbert, T., Vilar, J., Moreau, E., Freund, N., Lelievre-Pegorier, M., 1999. Nephron number: variability is the rule: causes and consequences. *Lab. Invest.* 79, 515–527.
- Mugford, J.W., Yu, J., Kobayashi, A., McMahon, A.P., 2009. High-resolution gene expression analysis of the developing mouse kidney defines novel cellular compartments within the nephron progenitor population. *Dev. Biol.* 333, 312–323.
- Packard, A., Georgas, K., Michos, O., Riccio, P., Cebrian, C., Combes, A.N., Ju, A., Ferrer-Vaquer, A., Hadjantonakis, A.K., Zong, H., Little, M.H., Costantini, F., 2013. Luminal mitosis drives epithelial cell dispersal within the branching ureteric bud. *Dev. Cell* 27, 319–330.
- Qian, H., Sheetz, M.P., Elson, E.L., 1991. Single particle tracking. Analysis of diffusion and flow in two-dimensional systems. *Biophys. J.* 60, 910–921.
- R Core Team, 2015. R: A language and environment for statistical computing. R Foundation for Statistical Computing, Vienna, Austria. (<https://www.R-project.org/>).
- Riccio, P., Cebrian, C., Zong, H., Hippenmeyer, S., Costantini, F., 2016. Ret and Etv4 promote directed movements of progenitor cells during renal branching morphogenesis. *PLoS Biol.* 14, e1002382.
- Shakya, R., Watanabe, T., Costantini, F., 2005. The role of GDNF/Ret signaling in ureteric bud cell fate and branching morphogenesis. *Dev. Cell* 8, 65–74.
- Srinivas, S., Goldberg, M.R., Watanabe, T., D'Agati, V., al-Awqati, Q., Costantini, F., 1999. Expression of green fluorescent protein in the ureteric bud of transgenic mice: a new tool for the analysis of ureteric bud morphogenesis. *Dev. Genet.* 24, 241–251.
- Wainwright, E.N., Wilhelm, D., Combes, A.N., Little, M.H., Koopman, P., 2015. ROBO2 restricts the nephrogenic field and regulates Wolffian duct-nephrogenic cord separation. *Dev. Biol.* 404, 88–102.
- Watanabe, T., Costantini, F., 2004. Real-time analysis of ureteric bud branching morphogenesis in vitro. *Dev. Biol.* 271, 98–108.